Effect of Particle Shape on the Flow of an Hourglass

Bo Fan,[1,3] Tivadar Pongó,[2,4,1] Raúl Cruz Hidalgo,[2] and Tamás Börzsönyi[1]
[1]Institute for Solid State Physics and Optics, HUN-REN Wigner Research Centre for Physics, P.O. Box 49, H-1525 Budapest, Hungary
[2]Física y Matemática Aplicada, Facultad de Ciencias, Universidad de Navarra, Pamplona, Spain
[3]Physical Chemistry and Soft Matter, Wageningen University and Research, Wageningen, The Netherlands
[4]Collective Dynamics Lab, Division of Natural and Applied Sciences, Duke Kunshan University, 215306, Kunshan, Jiangsu, China

(Received 17 March 2023; revised 7 November 2023; accepted 11 June 2024; published 31 July 2024)

The flow rate of a granulate out of a cylindrical container is studied as a function of particle shape for flat and elongated ellipsoids experimentally and numerically. We find a nonmonotonic dependence of the flow rate on the grain aspect ratio a/b. Starting from spheres the flow rate grows and has two maxima around the aspect ratios of $a/b \approx 0.6$ (lentil-like ellipsoids) and $a/b \approx 1.5$ (ricelike ellipsoids) reaching a flow rate increase of about 15% for lentils compared to spheres. For even more anisometric shapes ($a/b = 0.25$ and $a/b = 4$) the flow rate drops. Our results reveal two contributing factors to the nonmonotonic nature of the flow rate: both the packing fraction and the particle velocity through the orifice are nonmonotonic functions of the grain shape. Thus, particles with slightly nonspherical shapes not only form a better packing in the silo but also move faster through the orifice than spheres. We also show that the resistance of the granulate against shearing increases with aspect ratio for both elongated and flat particles; thus change in the effective friction of the granulate due to changing particle shape does not coincide with the trend in the flow rate.

DOI: 10.1103/PhysRevLett.133.058201

Flow of a granular material out of a container is a common process in everyday life, agriculture, and industrial operations. Typically, a granulate discharges through the orifice with a constant flow rate, independent of the filling height [1,2]. This feature was used when the hourglass was constructed as a time measuring device long ago, and it is very useful as the required flow rate can be easily set by simply choosing the appropriate orifice size. The flow rate changes with increasing orifice size as a power law function (Beverloo law [2–7]) and also depends on the internal friction of the granular material, which is changing with the surface roughness as well as the shape of the grains. Naturally, increasing particle roughness negatively impacts the flow rate, but it is much less obvious how it should change with grain shape. On one end of the spectrum, very irregular grains can get entangled during the discharge and flow less easily, but what should we expect from shapes that deviate only slightly from a sphere: ellipsoids with ricelike or lentil-like shapes?

Elongated or flat particles are observed to develop orientational ordering in a *shear flow*, with their smallest cross section facing almost in the flow direction [8–12]. The average orientation angle decreases with increasing grain anisometry, and, e.g., is around 10° for a ricelike ellipsoid with elongation $a/b = 3$. Naively, this would then suggest easier flow and thus faster flow rate through a constriction for simple elongated or flat ellipsoids than for spherical particles. However, taking a closer look at the dynamics of such particles in a shear flow, we observe that they perform irregular rotation as dictated by the shear stress related to the interaction with their neighbors. On average, they rotate slower when they are nearly parallel to the flow direction and rotate faster when they are perpendicular to it [9]. So during their rotation, they spend most of the time nearly parallel to the flow, which leads to the above-described average orientation. But as they rotate, neighboring particles actually get into conflict and hinder each other's motion. This leads to a nontrivial rheology for such types of granular materials.

Previous studies focusing on the fundamental question of the effect of the grain shape on the *rheology* of a granular material or *discharge rate from a silo* are mostly *numerical*. This is because discrete element model (DEM) simulations offer a straightforward way to systematically change the particle shape without changing the other parameters (microscopic surface friction, etc.). As for the *rheology*, recent DEM studies show that for frictional particles the effective friction μ_{eff} of the system is increasing with grain anisometry. This was found for spherocylinders in quasistatic shear flow for interparticle friction $\mu_p > 0.4$ [13], or in more dynamic inclined plane flows for $\mu_p \geq 0.5$ [14]. Similar observations were made in a simplified two-dimensional (2D) system [15]. Interestingly, for systems with lower interparticle friction ($\mu_p < 0.4$) a nonmonotonic tendency was found: starting from a spherical shape μ_{eff} first increases and then decreases with a/b. Focusing on previous DEM results on the *discharge of a 3D silo* with frictional grains one finds contradictory observations.

On one hand, Liu *et al.* found a reduced discharge rate for both elongated and flat ellipsoids compared to the case of spheres [16]; on the other hand, Li *et al.* reported a larger flow rate for round disks than for spheres [17]. In a recent work by Hesse *et al.* decreased and increased flow rate was found for elongated and flat ellipsoids compared to spheres, respectively [18]. Finally, for frictionless grains Langston *et al.* reported the same flow rate for spherocylinders and spheres [19].

To our best knowledge, so far no systematic *experimental* tests have been performed to measure how the discharge rate changes with particle shape when all other parameters (surface roughness, density, hardness, etc.) are identical. For rodlike shapes, a flow rate decrease was detected with increasing aspect ratio comparing two samples of glass rods with two samples of plastic rods [20].

In this Letter, we investigate experimentally the effect of particle shape on the flow rate of a granulate out of a container. We use custom-made particles which differ only in shape, while their volume and all other parameters are identical. We also test the resistance of our samples against quasistatic shearing. Our experiments are complemented with discrete element modelling (DEM).

In the experiments, we used nine different samples of polyoxymethylene rotational ellipsoids (produced by injection molding by Yuyao Strong Co., China [21]). Each sample contained 50 000 identical particles; see Fig. 1(a) for photographs of the particles and their characteristic dimensions. The flow rate experiments were performed

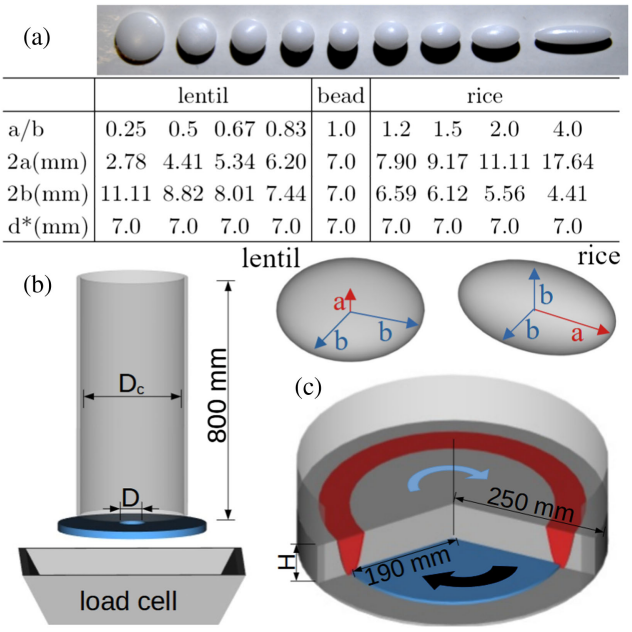

	lentil				bead	rice			
a/b	0.25	0.5	0.67	0.83	1.0	1.2	1.5	2.0	4.0
2a(mm)	2.78	4.41	5.34	6.20	7.0	7.90	9.17	11.11	17.64
2b(mm)	11.11	8.82	8.01	7.44	7.0	6.59	6.12	5.56	4.41
d*(mm)	7.0	7.0	7.0	7.0	7.0	7.0	7.0	7.0	7.0

FIG. 1. (a) Photographs and dimensions of the particles. All particles are rotational ellipsoids; they have the same volume, equivalent to the volume of a sphere with the diameter $d^* = 7$ mm. (b),(c) Schematic diagrams of the experimental setups: silo and cylindrical split-bottom shear cell.

using an acrylic cylinder with an inner diameter of either $D_c = 172$ mm or 144 mm and a length of 800 mm with an orifice at the bottom with adjustable diameter D [see Fig. 1(b)]. The granulate was filled into the cylinder manually, and after opening the orifice, we recorded the flow rate by measuring the weight of the discharged mass with a load cell. In a complementary experiment, we measured the resistance of the granulate against shearing in a cylindrical split-bottom shear cell [see Fig. 1(c)]. Here, the middle part of the sample was rotated with a rotating plate under it and thereby stationary shear was applied in the shear zone [see red region in Fig. 1(c)] between the moving and standing regions. The applied torque was measured during stationary shearing.

The DEM implementation handles nonspherical particles and their contact interaction using the superquadric equation [22]. In particular, we employed a self-written GPU-NVIDIA implementation as a parallelization procedure [23] based on [24,25], which allowed the examination of system sizes comparable with the experiments. A superquadric is defined by the length of its half axes a, b, c, and the blockiness parameters n_1 and n_2. To mimic the experiments, the parameters $n_1 = n_2 = 2$ were set, representing ellipsoids. Moreover, the values of a, $b \equiv c$ were the same as those of the experimental particles. Complementarily, additional simulations were also done with triaxial ellipsoids ($a \neq b \neq c$) to check the generality of the results [26]. In all the cases, the system is composed of $N = 50\,000$ monodisperse superquadrics, of the same equivalent diameter d^*. Polyoxymethylene has relatively low surface friction; therefore in the simulations presented here we use an interparticle friction coefficient of $\mu = 0.3$ [27]. After defining the particle-particle and particle-wall contact forces, the DEM computes the movement of each particle; see more details in Supplemental Material [26]. For the computation of the density, velocity, and stress macroscopic fields, we have taken advantage of a useful coarse-graining technique, described in [28–31].

The evolution of the normalized flow rate obtained in both experiments and simulations is presented as a function of the mass in the cylinder during the discharge process in Fig. 2. The mass in the cylinder is normalized by the mass corresponding to the filling height of D_c. The datasets are normalized by the average flow rate of beads. The average flow rate is calculated using data in the middle of the discharge process, i.e., in the range of $1.4 < m/m_{D_c} < 2.8$. Similar plots were obtained in the smaller silo ($D_c = 144$ mm). We mention that for a narrow cylinder, a surge is observed at the end of the discharge process for a certain range of the orifice diameter [32]. For most of our current measurements, there was no surge; for those where a surge occurs, we average the flow rate before the surge.

We summarize our findings by plotting the average flow rate as a function of the particle aspect ratio in

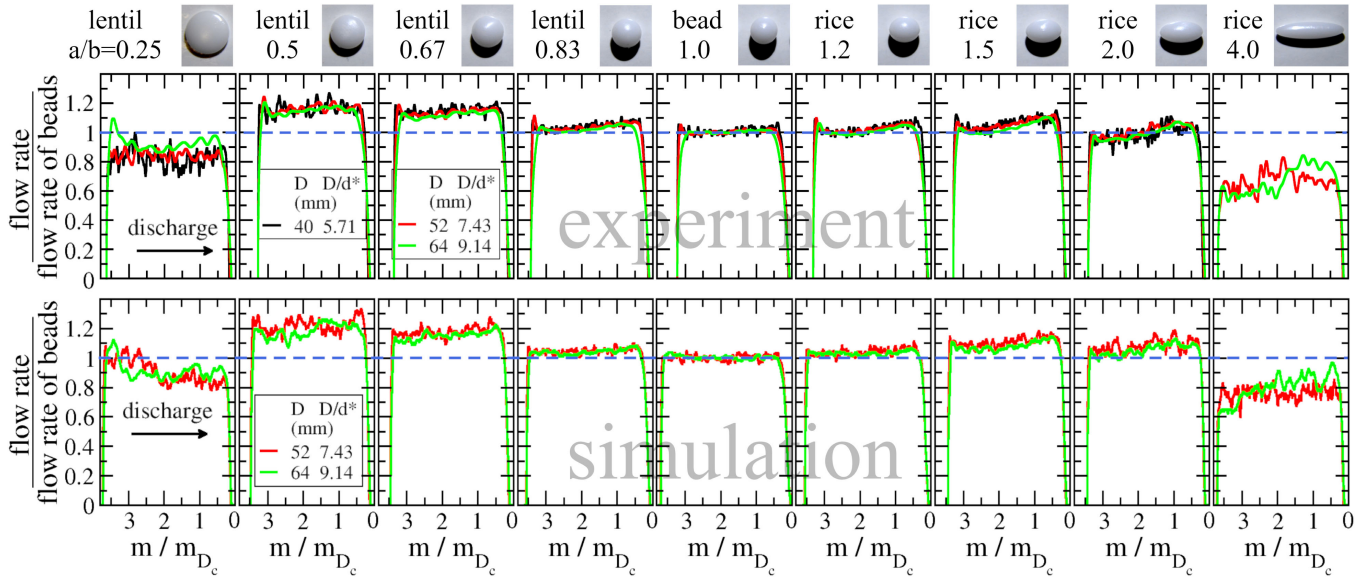

FIG. 2. Normalized flow rate as a function of the mass in the cylinder for all nine ellipsoidal samples during the discharge process. The average flow rate for beads is calculated in the range of $1.4 < m/m_{D_c} < 2.8$. Top row: experimental data obtained in the cylinder with $D_c = 172$ mm with orifice sizes of $D = 40$, 52, and 64 mm. Each curve corresponds to the average of five measurements. Bottom row: numerical results for the same setting. The curves correspond to a single run except for the cases of $a/b = 0.25$ and $a/b = 4.0$ for which four runs are averaged.

Figs. 3(a) and 3(d). Starting from the spherical shape and going toward lentil-like shapes we first find a clear increase of the flow rate having a maximum around the aspect ratio of $a/b \approx 0.6$ and then a strong decrease for the grains with $a/b = 0.25$. When we go in the direction of elongated grains, around the aspect ratio of about $a/b \approx 1.5$ we again find a peak, but this is smaller than for the case of lentils, and the effect is more pronounced for the DEM data than in

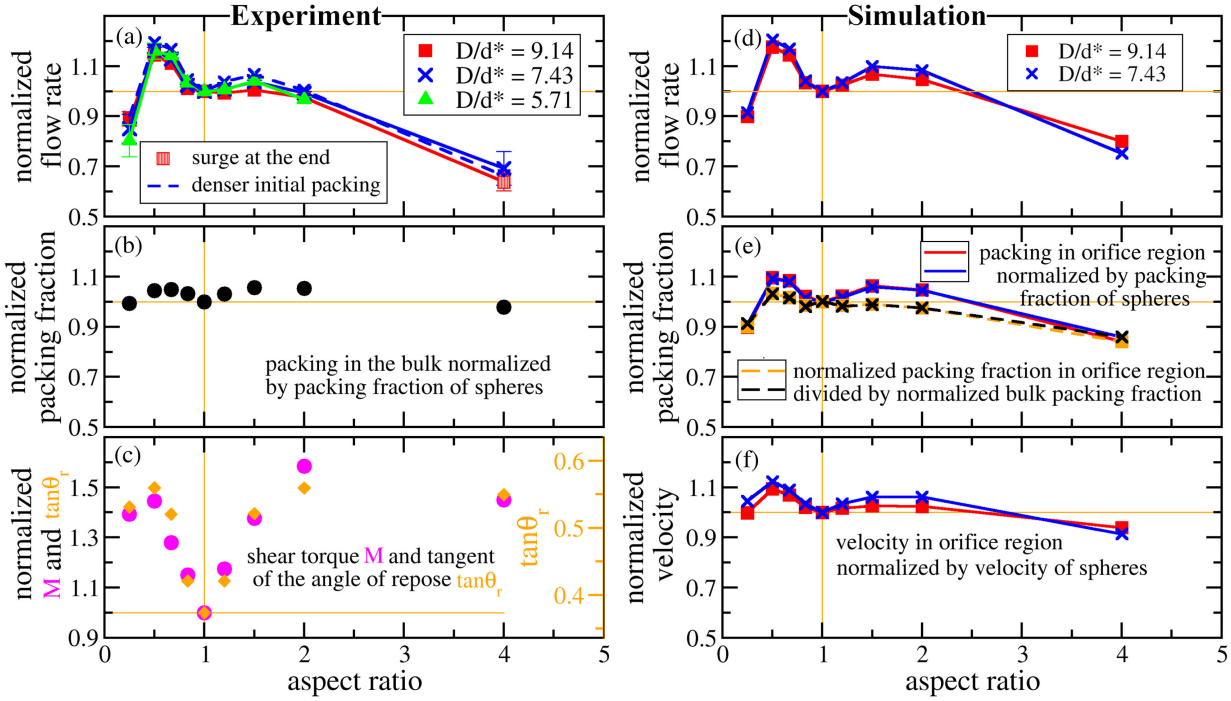

FIG. 3. Experimental results: (a) average flow rate, (b) static packing fraction, and (c) shear torque and tangent of the angle of repose as a function of particle aspect ratio. All quantities normalized by the value obtained for beads. The average flow rate was obtained by averaging the data in the range of $1.4 < m/m_{D_c} < 2.8$. Numerical results: (d) average flow rate, (e) packing fraction, and (f) velocity as a function of aspect ratio.

experiments [compare Figs. 3(a) and 3(d)]. Above the aspect ratio of $a/b = 2$ the flow rate clearly decreases. In Fig. 3(a) we also included a curve obtained in experiments with denser initial packing, which shows the same trend as the other curves. A recent work has highlighted the importance of the shape of the orifice rim on the flow rate [33]; thus we performed further experiments with a conical orifice that also show the same trend. Details about the measurements with denser initial packing and a conical orifice can be found in the Supplemental Material [26]. We also mention that the above results are consistent with other experimental observations in a conical hopper, where the discharge rate is found to be larger for lentil-like grains ($a/b = 0.6$) and slightly lower for ricelike grains ($a/b = 3$) compared to spheres [34].

In order to explore the nonmonotonic nature of the flow rate curves [Figs. 3(a) and 3(d)], we first investigate whether this can be rather related to variations in packing fraction or grain velocities through the orifice.

In the *experiments*, we can measure the bulk packing fraction of the initial state of each sample by measuring the weight of the sample in dry state and then submerged in water. As we see in Fig. 3(b) the initial packing in the cylinder slightly depends on the grain shape with a nonmonotonic dependence for both lentil-like and ricelike shapes. The densest packings correspond to aspect ratios $a/b = 0.5$ and $a/b = 2$, and are about 6% denser than the packing of spheres. A very similar dataset (not shown here) is obtained from our DEM simulations. All this is consistent with the results of earlier numerical calculations predicting similar shape dependence for the random close packed density [35] and poured density [36] for both elongated and flat ellipsoids. Altogether, for the case of lentils the modulation of the initial bulk packing fraction with shape is small compared to the changes in flow rate, so it does not fully explain the flow rate behavior [Figs. 3(a) and 3(d)].

In the *numerical simulations*, we can quantify the packing fraction as well as the velocity of the grains in the orifice region [see Figs. 3(e) and 3(f)]. As we see, they both show nonmonotonic shape dependence, and for the friction coefficient used here ($\mu = 0.3$) they give approximately an equal contribution to form the trend observed in the flow rate. We mention that for $\mu = 0.5$ the contribution of grain velocity becomes stronger (see Supplemental Material). Analyzing the data of the packing fraction first [Fig. 3(e)], we find that dividing the normalized packing fraction in the orifice region by the normalized bulk packing fraction the resulting curve becomes nearly shape independent in the range of $0.5 \leq a/b \leq 2$. This means, that the flow does not significantly impact the packing in the orifice region for slightly elongated or flat ellipsoids, so the two peaks on the packing fraction curves basically come from the peaks in the bulk packing fraction. Focusing on the nonmonotonic trend of the particle velocity, we plot

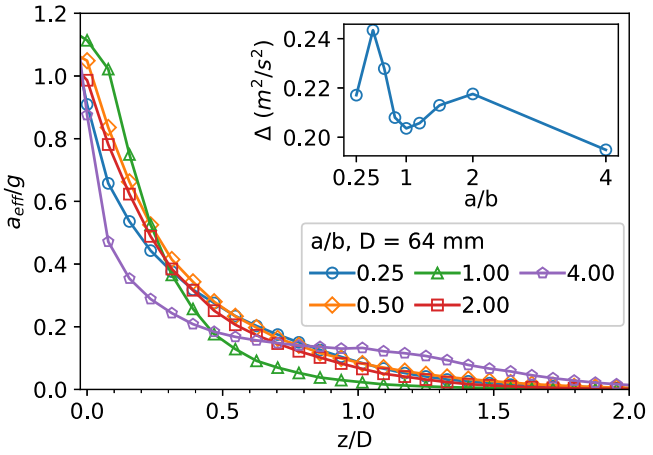

FIG. 4. Average acceleration of grains in the cylindrical region of diameter D above the orifice normalized by gravity as a function of the normalized distance z/D from the orifice. The inset shows $\Delta = v_{\text{exit}}^2/2$ at the orifice as a function of the aspect ratio.

the average acceleration above the orifice as a function of the distance from the orifice in Fig. 4. Far from the orifice, the velocity and acceleration of all types of grains are negligible. Interestingly, grains with nonspherical shape start accelerating from a higher position than the spheres, but as they get close to the orifice their acceleration becomes slightly smaller (compared to the case of spheres). Recovering the analysis done in [6], the vertical acceleration profile reads as $a_{\text{eff}}(z) = dv_z/dt = v_z dv_z/dz$. Thus, a test particle coming downward in the center, far from the orifice, will gain v_{exit} vertical velocity arriving at the orifice level, based on the integral $\Delta = \int_0^\infty a_{\text{eff}}(z)dz = v_{\text{exit}}^2/2$. The inset of Fig. 4 illustrates Δ as a function of particle aspect ratio a/b. Remarkably, it resembles the nonmonotonic dependence of the vertical velocity appearing in Fig. 3(f). Additionally, we also looked into the details of particle orientations in the orifice region. The analysis indicates that the nonsphericity significantly impacts the particle orientation and ordering with respect to flow (for details, see the Supplemental Material [26]). Interestingly, we find that for lentils and for short rice grains the flow rate and apparent particle size anticorrelate, i.e., particles with a smaller cross section toward the orifice display a higher flow rate.

Finally, coming back to the experimental data, we analyze how the resistance of the material against shearing is changing with grain shape, and whether this correlates with the flow rate behavior. We quantify this by measuring the shear torque needed for a stationary quasistatic rotation of the sample in the split-bottom shear cell. The normalized shear torque is presented as a function of the aspect ratio in Fig. 3(c). The data were obtained using samples with the volume of 7 l corresponding to a filling height of $H \approx 3.5$ cm. The data were normalized first by the weight of the sample and then by the normalized shear torque

obtained for beads. As we see both elongated and flat shapes are characterized by an increased shear resistance compared to the case of spheres. The increase in the shear torque reaches about 50% for both ricelike and lentil-like ellipsoids, with aspect ratios of $a/b = 2$ and 0.5, respectively. The increasing tendency is in accordance with our previous numerical findings on elongated shapes in simple shear [13] and inclined plane flow [14], as well as with the tangent of the angle of repose ($\tan\theta_r$), which is also presented in Fig. 3(c). The data for $\tan\theta_r$ were obtained in a quasi-two-dimensional cell [26,37] as an other measure to characterize the frictional property of the granulate. We emphasize that the data in Fig. 3(c) evidences larger bulk friction for both elongated and flat grains compared to the case of spherical particles, which would suggest smaller flow rate through a constriction for such particles. This is not in line with our observations on the flow rate, as described above. Thus, the trend in the flow rate can not be explained by the shape dependence of the shear resistance and that of the angle of repose.

In summary, we find a surprising nonmonotonic behavior of the silo flow rate as a function of grain shape for rotational and triaxial ellipsoids. Slightly nonspherical particles discharge faster than spheres, the effect is stronger for lentil-like shapes than for ricelike shapes. Analyzing the packing fraction and grain velocity in the orifice region, we find that they both contribute to the nonmonotonic tendency of the flow rate. The contribution of the packing fraction mainly originates from the nonmonotonic shape dependence of the bulk packing fraction, while the contribution of grain velocity is related to two factors: (i) the height above the orifice line at which grains start accelerating (this is larger for nonspherical grains than for spheres), and (ii) the rate at which they speed up, which certainly depends on the dissipation in the region right above the orifice. The optimum of these two effects is found for the slightly flat lentil-like shapes, which produce the largest discharge rate in the silo. Finally, the resistance of the granulate against shearing considerably increases for both lentil-like and ricelike particles (compared to spheres); thus its trend does not coincide with the trend of the flow rate.

Acknowledgments—The authors acknowledge financial support from the European Union by Horizon 2020 Marie Skłodowska-Curie grant "CALIPER" (No. 812638) and COST action "ON-DEM" (No. CA22132). We are thankful for the discussions with J. A. Dijksman and J. van der Gucht and to V. Kenderesi for technical assistance. R. C. H. acknowledges the Ministerio de Ciencia e Innovación (Spanish Government) Grant PID2020–114839 GB-I00 funded by MCIN/AEI/10.13039/501100011033. T. P. acknowledges support by the Startup Grant from DKU. The Collective Dynamics Lab is partly sponsored by a philanthropic gift. B. F. and T. P. should be considered co-first authors.

[1] R. T. Fowler and J. R. Glastonbury, Chem. Eng. Sci. **10**, 150 (1959).
[2] W. A. Beverloo, H. A. Leniger, and J. van de Velde, Chem. Eng. Sci. **15**, 260 (1961).
[3] R. M. Nedderman, U. Tüzün, S. B. Savage, and G. T. Houlsby, Chem. Eng. Sci. **37**, 1597 (1982).
[4] C. Mankoc, A. Janda, R. Arévalo, J. M. Pastor, I. Zuriguel, A. Garcimartín, and D. Maza, Granular Matter **9**, 407 (2007).
[5] J. E. Hilton and P. W. Cleary, Phys. Rev. E **84**, 011307 (2011).
[6] S. M. Rubio-Largo, A. Janda, D. Maza, I. Zuriguel, and R. C. Hidalgo, Phys. Rev. Lett. **114**, 238002 (2015).
[7] C. A. Calderón, M. C. V. Olivares, R. O. Unac, and A. M. Vidales, Powder Technol. **320**, 43 (2017).
[8] T. Börzsönyi, B. Szabó, G. Törös, S. Wegner, J. Török, E. Somfai, T. Bien, and R. Stannarius, Phys. Rev. Lett. **108**, 228302 (2012).
[9] T. Börzsönyi, B. Szabó, S. Wegner, K. Harth, J. Török, E. Somfai, T. Bien, and R. Stannarius, Phys. Rev. E **86**, 051304 (2012).
[10] T. Börzsönyi and R. Stannarius, Soft Matter **9**, 7401 (2013).
[11] T. Börzsönyi, E. Somfai, B. Szabó, S. Wegner, P. Mier, G. Rose, and R. Stannarius, New J. Phys. **18**, 093017 (2016).
[12] M. Boton, E. Azéma, N. Estrada, F. Radjaï, and A. Lizcano, Phys. Rev. E **87**, 032206 (2013).
[13] D. B. Nagy, P. Claudin, T. Börzsönyi, and E. Somfai, New J. Phys. **22**, 073008 (2020).
[14] R. C. Hidalgo, B. Szabó, K. Gillemot, T. Börzsönyi, and T. Weinhart, Phys. Rev. Fluids **3**, 074301 (2018).
[15] M. Trulsson, J. Fluid Mech. **849**, 718 (2018).
[16] S. D. Liu, Z. Y. Zhou, R. P. Zou, D. Pinson, and A. B. Yu, Powder Technol. **253**, 70 (2014).
[17] J. Li, P. A. Langston, C. Webb, and T. Dyakowski, Chem. Eng. Sci. **59**, 5917 (2004).
[18] R. Hesse, F. Krull, and S. Antonyuk, Powder Technol. **393**, 559 (2021).
[19] P. A. Langston, M. A. Al-Awamleh, F. Y. Fraige, and B. N. Asmar, Chem. Eng. Sci. **59**, 425 (2004).
[20] A. Ashour, S. Wegner, T. Trittel, T. Börzsönyi, and R. Stannarius, Soft Matter **13**, 402 (2017).
[21] T. Borzsonyi, G. Pinzon, M. A. Hanif, T. Trittel, R. Stannarius, C. Klopp, CaliParticles: A benchmark standard for experiments in granular materials, Zenodo (2024), 10.5281/zenodo.10517970.
[22] G. Lu, J. R. Third, and C. R. Müller, Chem. Eng. Sci. **127**, 425 (2015).
[23] T. Pongó, M. A. Hanif, D. Maza, D. van der Meer, and R. C. Hidalgo, Powder Technol. (to be published).
[24] A. Podlozhnyuk, S. Pirker, and C. Kloss, Comput. Part. Mech. **4**, 101 (2017).
[25] H. A. Navarro and M. P. de Souza Braun, Powder Technol. **246**, 707 (2013).
[26] See Supplemental Material at http://link.aps.org/supplemental/10.1103/PhysRevLett.133.058201 for additional experimental and numerical data.
[27] J. L. Laursen, I. M. Sivebaek, L. W. Christoffersen, M. Papsoee, M. E. Vigild, P. Brondsted, and A. Horsewell, Wear **267**, 2294 (2009).
[28] M. Babic, Int. J. Eng. Sci. **35**, 523 (1997).

[29] I. Goldhirsch, Granular Matter **12**, 239 (2010).
[30] T. Weinhart, R. Hartkamp, A. Thornton, and S. Luding, Phys. Fluids **25**, 070605 (2013).
[31] R. Artoni and P. Richard, Phys. Rev. E **91**, 032202 (2015).
[32] T. Pongó, B. Fan, D. Hernández-Delfin, J. Török, R. Stannarius, R. C. Hidalgo, and T. Börzsönyi, New J. Phys. **24**, 103036 (2022).
[33] J. Wiacek, J. Horabik, M. Molenda, P. Parafiniuk, M. Banda, and M. Stasiak, Sci. Rep. **13**, 669 (2023).
[34] M. A. Hanif, T. Pongó, D. Maza, R. C. Hidalgo, and D. van der Meer (to be published).
[35] A. Donev, I. Cisse, D. Sachs, E. A. Variano, F. H. Stillinger, R. Connelly, S. Torquato, and P. M. Chaikin, Science **303**, 990 (2004).
[36] J. Q. Gan, Z. Y. Zhou, and A. B. Yu, Powder Technol. **335**, 327 (2018).
[37] Y. Fan, Y. Boukerkour, T. Blanc, P. B. Umbanhowar, J. M. Ottino, and R. M. Lueptow, Phys. Rev. E **86**, 051305 (2012).